Benchmark Solutions For Transport In d-Dimensional Markov Binary Mixtures

C. Larmier, F.-X. Hugot, F. Malvagi, A. Mazzolo, A. Zoia

M&C 2017 - International Conference on Mathematics & Computational Methods Applied to Nuclear Science & Engineering, Jeju, Korea, April 16-20, 2017, on USB (2017)

Benchmark solutions for transport in d-dimensional Markov binary mixtures

Coline Larmier,* François-Xavier Hugot,* Fausto Malvagi,* Alain Mazzolo,* Andrea Zoia,*

*Den-Service d'études des réacteurs et de mathématiques appliquées (SERMA), CEA, Université Paris-Saclay, F-91191, Gif-sur-Yvette, France
andrea.zoia@cea.fr*

Abstract - *Particle transport in random media obeying a given mixing statistics is key in several applications in nuclear reactor physics and more generally in diffusion phenomena emerging in physics and life sciences. Exact solutions for the ensemble-averaged physical observables are hardly available, and several effective models have been thus developed, providing a compromise between the accurate treatment of the disorder-induced spatial correlations and the computational time. In order to validate these models, it is mandatory to resort to reference solutions. We extend the pioneering work by Adams, Larsen and Pomraning [1] (recently revisited by Brantley [2]) by considering a series of benchmark configurations for mono-energetic and isotropic transport through Markov binary mixtures in dimension d. The stochastic media are generated by resorting to Poisson random tessellations in 1d slab, 2d extruded, and full 3d geometry. For each realization, particle transport is performed by resorting to Monte Carlo simulation. The distributions of the transmission and reflection coefficients on the free surfaces of the geometry are subsequently estimated, and the average values over the ensemble of realizations are computed. Reference solutions for the benchmark have never been provided before for two- and three-dimensional Poisson tessellations, and the results presented in this paper might thus be useful in order to validate fast but approximated models for particle transport in Markov stochastic media, such as the celebrated Chord Length Sampling algorithm.*

I. INTRODUCTION

Linear transport through heterogeneous and disordered media emerges in several applications in nuclear science and engineering. Examples are widespread and concern for instance neutron diffusion in pebble-bed reactors or randomly mixed immiscible materials [3, 4], and inertial confinement fusion [5]. The key goal of particle transport theory in stochastic media consists in deriving a formalism for the description of the ensemble-averaged angular particle flux $\langle\varphi(\mathbf{r},\boldsymbol{\omega})\rangle$, where $\varphi(\mathbf{r},\boldsymbol{\omega})$ solves the linear (single-speed) Boltzmann equation

$$\boldsymbol{\omega}\cdot\nabla\varphi+\Sigma(\mathbf{r})\varphi=\int\Sigma_s(\boldsymbol{\omega}'\rightarrow\boldsymbol{\omega},\mathbf{r})\varphi(\mathbf{r},\boldsymbol{\omega}')d\boldsymbol{\omega}'+S, \quad (1)$$

$\mathbf{r}$ and $\boldsymbol{\omega}$ denoting the position and direction variables, respectively, $\Sigma(\mathbf{r})$ being the total cross section, $\Sigma_s(\boldsymbol{\omega}'\rightarrow\boldsymbol{\omega},\mathbf{r})$ the differential scattering cross section, and $S=S(\mathbf{r},\boldsymbol{\omega})$ the source term. For isotropic scattering, the differential scattering cross section simplifies to $\Sigma_s(\boldsymbol{\omega}'\rightarrow\boldsymbol{\omega},\mathbf{r})=\Sigma_s(\mathbf{r})/\Omega_d$, where Ω_d is the surface area of the unit sphere in dimension d. The stochastic nature of particle transport stems from the materials composing the traversed medium being randomly distributed according to some statistical law. Hence, the quantities $\Sigma(\mathbf{r})$, $\Sigma_s(\boldsymbol{\omega}'\rightarrow\boldsymbol{\omega},\mathbf{r})$ and $S(\mathbf{r},\boldsymbol{\omega})$ are in principle random variables. A widely adopted model of random media is the so-called binary stochastic mixing, where only two immiscible materials (say α and β) are present [3]. Then, by averaging Eq. (1) over realizations having material α at $\mathbf{r}$, we obtain the following equation for $\langle\varphi_\alpha(\mathbf{r},\boldsymbol{\omega})\rangle$

$$\begin{aligned}[\boldsymbol{\omega}\cdot\nabla+\Sigma_\alpha]\,p_\alpha\langle\varphi_\alpha\rangle=\tfrac{p_\alpha\Sigma_{s,\alpha}}{\Omega_d}\int\langle\varphi_\alpha(\mathbf{r},\boldsymbol{\omega}')\rangle d\boldsymbol{\omega}'+p_\alpha S_\alpha\\+p_{\beta,\alpha}\langle\varphi_{\beta,\alpha}\rangle-p_{\alpha,\beta}\langle\varphi_{\alpha,\beta}\rangle\end{aligned} \quad (2)$$

where $p_i(\mathbf{r})$ is the probability of finding the material of index i at position $\mathbf{r}$. Here $p_{i,j}=p_{i,j}(\mathbf{r},\boldsymbol{\omega})$ denotes the probability per unit length of crossing the interface from material i to material j for a particle located at $\mathbf{r}$ and travelling in direction $\boldsymbol{\omega}$, and $\langle\varphi_{i,j}\rangle$ denoting the angular flux averaged over those realizations where there is a transition from material i to material j for a particle located at $\mathbf{r}$ and travelling in direction $\boldsymbol{\omega}$. The cross sections Σ_α and $\Sigma_{s,\alpha}$ are those of material α. The equation for $\langle\varphi_\beta(\mathbf{r},\boldsymbol{\omega})\rangle$ is immediately obtained from Eq. (2) by permuting the indexes α and β.

The set of equations in Eq. (2) can be shown to form an infinite hierarchy [3, 4]. Generally speaking, it is therefore necessary to introduce a closure formula, depending on the underlying mixing statistics. The celebrated Levermore-Pomraning model assumes for instance $\langle\varphi_{\alpha,\beta}\rangle=\langle\varphi_\alpha\rangle$ for homogeneous Markov mixing statistics [3], which is defined by

$$p_{i,j}(\mathbf{r},\boldsymbol{\omega})=\frac{p_i}{\Lambda_i(\boldsymbol{\omega})}, \quad (3)$$

depending on the starting position alone, where $\Lambda_i(\boldsymbol{\omega})$ is the mean chord length for trajectories crossing material i in direction $\boldsymbol{\omega}$. Several generalisations of this model have been later proposed, including higher-order closure schemes [3]. In parallel, Monte Carlo algorithms such as the Chord Length Sampling have been conceived in order to address the Levermore-Pomraning model, and have been further extended so as to include partial memory effects due to correlations for particles crossing back and forth the same materials [5]. Their common feature is that they allow a simpler, albeit approximate, treatment of transport in stochastic mixtures, which might be convenient in practical applications.

In order to assess the accuracy of the various approximate models it is therefore mandatory to compute reference solutions for the exact Eqs. (2). Such solutions can be obtained in the following way: first, a realization of the medium is

sampled from the underlying mixing statistics; then, the linear transport equations corresponding to this realization are solved by either deterministic or Monte Carlo methods, and the physical observables of interest are determined; this procedure is repeated many times so as to create a sufficiently large collection of realizations, and ensemble averages are finally taken for the physical observables. For this purpose, a number of benchmark problems for Markov mixing have been proposed in the literature so far [1, 4, 2], with focus exclusively on $1d$ geometries, either of the rod or slab type.

In this work we will revisit the classical benchmark problem proposed by Adams, Larsen and Pomraning for transport in stochastic media [1]. We will present reference solutions obtained by Monte Carlo particle transport simulation through $1d$ slab, $2d$ extruded and $3d$ tessellations of a finite-size box with Markov mixing. We will compute the particle flux $\langle\varphi\rangle$, the transmission coefficient $\langle T\rangle$ and the reflection coefficient $\langle R\rangle$ by taking ensemble averages over the realizations; the dispersion of the physical observables around their average values will be assessed by evaluating their full distributions. Benchmark solutions for transport in $2d$ extruded and $3d$ tessellations have never been addressed before.

II. BENCHMARK SPECIFICATIONS

The benchmark specifications for our work are essentially taken from those originally proposed in [1, 4], and later extended in [2]. We consider single-speed linear particle transport through a stochastic binary medium with homogeneous Markov mixing. The medium is non-multiplying, with isotropic scattering. The geometry consists of a cubic box of side $L = 10$, with reflective boundary conditions on all sides of the box except two opposite faces (say those perpendicular to the x axis), where leakage boundary conditions are imposed: particles that leave the domain through these faces can not re-enter. Lengths are expressed in arbitrary units. In [1] and [4], system sizes $L = 0.1$ and $L = 1$ were also considered, but in this work we will focus on the case $L = 10$, which leads to more physically relevant configurations. Two kinds of non-stochastic sources have been considered in [2], namely, an imposed normalized incident angular flux on the leakage surface at $x = 0$ (with zero interior sources), or a distributed homogeneous and isotropic normalized interior source (with zero incident angular flux on the leakage surfaces). The benchmark configurations pertaining to the former kind of source have been conventionally called *suite* I, whereas those pertaining to the latter have been called *suite* II [2]. In this work, we will present the simulation results for *suite* I, and we refer the reader to a companion work [**?**] for those of *suite* II. The material properties for the Markov mixing are entirely defined by assigning the average chord length for each material $i = \alpha, \beta$, namely Λ_i, which in turn allows deriving the homogeneous probability p_i of finding material i at an arbitrary location within the box, namely, $p_i = \Lambda_i/(\Lambda_i + \Lambda_j)$. The material probability p_i defines the volume fraction for material i. The cross sections for each material will be denoted as customary Σ_i for the total cross section and $\Sigma_{s,i}$ for the scattering cross section. The average number of particles surviving a collision in material i will be denoted by $c_i = \Sigma_{s,i}/\Sigma_i \leq 1$. The physical parameters for the benchmark configurations are recalled in Tabs. I and II: three cases (numbered 1, 2 and 3) are considered, each containing three sub-cases (noted a, b and c). The case numbers correspond to varying the materials, whereas the sub-cases represents varying ratios of c_i for each material.

Case	Σ_α	Λ_α	Σ_β	Λ_β
1	10/99	99/100	100/11	11/100
2	10/99	99/10	100/11	11/10
3	2/101	101/20	200/101	101/20

TABLE I. Material parameters for the three cases of the benchmark configurations.

Sub-case	a	b	c
c_α	0	1	0.9
c_β	1	0	0.9

TABLE II. Material parameters for the three sub-cases of the benchmark configurations.

The physical observables of interest for the proposed benchmark will be the ensemble-averaged outgoing particle currents $\langle J\rangle$ on the two surfaces with leakage boundary conditions, and the ensemble-averaged scalar particle flux $\langle\varphi(x)\rangle = \langle\int\int\int\varphi(\mathbf{r},\omega)d\omega dydz\rangle$ along $0 \leq x \leq L$. For the *suite* I configurations, the outgoing particle current on the side opposite to the imposed current source will represent the ensemble-averaged transmission coefficient, namely, $\langle T\rangle = \langle J_{x=L}\rangle$, whereas the outgoing particle current on the side of the current source will represent the ensemble-averaged reflection coefficient, namely, $\langle R\rangle = \langle J_{x=0}\rangle$.

III. POISSON GEOMETRIES

Poisson geometries form a prototype process of isotropic stochastic tessellations: a portion of a d-dimensional space is partitioned by randomly generated $(d-1)$-dimensional hyper-planes drawn from an underlying Poisson process [6]. An explicit construction amenable to Monte Carlo realizations for two-dimensional homogeneous and isotropic Poisson geometries of finite size has been established in [7]. A generalization of this algorithm to three-dimensional (and in principle d-dimensional) domains has recently been proposed [8], based on a spatial tessellation of the d-hypersphere of radius R centered at the origin by a random number m of $(d-1)$-hyperplanes with random orientation and position. The number m of $(d-1)$-hyperplanes is sampled from a Poisson distribution with parameter $\rho R\mathcal{A}_d(1)/\mathcal{V}_{d-1}(1)$. Here $\mathcal{A}_d(1) = 2\pi^{d/2}/\Gamma(d/2)$ denotes the surface of the d-dimensional unit sphere ($\Gamma(a)$ being the Gamma function), $\mathcal{V}_d(1) = \pi^{d/2}/\Gamma(1+d/2)$ denotes the volume of the d-dimensional unit sphere, and ρ is the arbitrary density of the tessellation, carrying the units of an inverse length.

The algorithm for the $1d$ slab tessellations is recalled

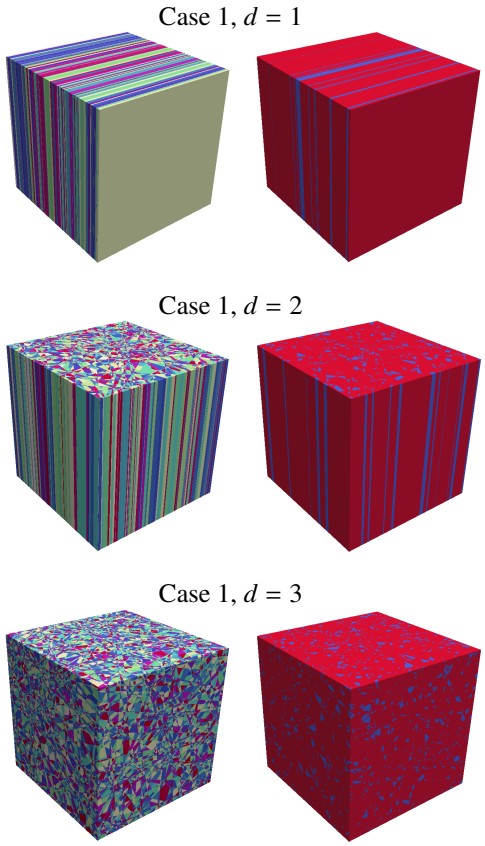

Fig. 1. Examples of realizations of Poisson geometries corresponding to the benchmark specifications for the $1d$ slab tessellations (top), $2d$ extruded tessellations (middle) and $3d$ tessellations (bottom), before (left) and after (right) attributing the material label. Red denotes label α and blue denotes label β. For case 1, $p_\alpha = 0.9$.

in [1], based on the Poisson process on the line. For the $2d$ extruded tessellations, we begin by creating an isotropic Poisson tessellation of a square of side L, according to the algorithm detailed in [9]. By construction, the polygons defined by the intersection of random lines drawn according to this method are convex. Once the square has been tessellated, the full geometrical description for the cube is simply achieved by extruding the random polyhedra (which lie on the $x - y$ plane) along the orthogonal z axis (see Fig. 1).

Let us now focus on $3d$ tessellations [10]. We denote by R the radius of the sphere circumscribed to the cube, and suppose that the cube is centered in the origin O. We start again by sampling a random number of points m from a Poisson distribution of parameter $4\rho R$, where we have used $\mathcal{A}_3(1)/\mathcal{V}_2(1) = 4$. Then we generate the planes that will cut the cube. We choose a radius r uniformly in the interval $[0, R]$ and then sample two additional parameters, namely, ξ_1 and ξ_2, from two independent uniform distributions in the interval $[0, 1]$. A unit vector $\mathbf{n} = (n_1, n_2, n_3)^T$ is generated, with components $n_1 = 1 - 2\xi_1$, $n_2 = \sqrt{1 - n_1^2}\cos(2\pi\xi_2)$, and $n_3 = \sqrt{1 - n_1^2}\sin(2\pi\xi_2)$. Let now $\mathbf{M}$ be the point such that $\mathbf{OM} = r\mathbf{n}$. The random plane will finally obey $n_1 x + n_2 y + n_3 z = r$, passing trough $\mathbf{M}$ and having normal vector $\mathbf{n}$. The procedure is iterated until m random planes have been generated. The polyhedra defined by the intersection of such random planes are convex (see Fig. 1).

Poisson geometries satisfy a Markov property: for domains of infinite size, arbitrary drawn lines will be cut by the $(d-1)$-surfaces of the d-polyhedra into segments whose lengths ℓ are exponentially distributed, i.e., $P(\ell) = \rho e^{-\rho\ell}$, with average $\langle\ell\rangle = \int \ell P(\ell) d\ell = 1/\rho$ [6]. The quantity $\Lambda = 1/\rho$ intuitively defines the correlation length of the Poisson geometry, i.e, the typical linear size of a volume composing the random tessellation.

Binary Markov mixtures required for the benchmark specifications are obtained as follows: first, a d-dimensional Poisson tessellation is constructed as described above. Then, each polyhedron of the geometry is assigned a material composition by formally attributing a distinct 'label' (also called 'color'), say 'α' or 'β', with associated complementary probabilities p_α and $p_\beta = 1 - p_\alpha$. Adjacent polyhedra sharing the same label are finally merged. This gives rise to (generally) non-convex α and β clusters, each composed of a random number of convex polyhedra. The statistical features of Poisson binary mixtures, including percolation probabilities and exponents, have been previously addressed in [9] for $2d$ geometries and in [10] for $3d$ geometries. It can be shown that the average chord length Λ_α through clusters with composition α is related to the correlation length Λ of the geometry via $\Lambda = (1-p_\alpha)\Lambda_\alpha$, and for Λ_β we similarly have $\Lambda = p_\alpha\Lambda_\beta$. This yields $1/\Lambda_\alpha + 1/\Lambda_\beta = 1/\Lambda$, and we recover

$$p_\alpha = \frac{\Lambda}{\Lambda_\beta} = \frac{\Lambda_\alpha}{\Lambda_\alpha + \Lambda_\beta}. \tag{4}$$

Thus, based on the formulas above, and using $\rho = 1/\Lambda$, the parameters of the colored Poisson geometries corresponding to the benchmark specifications provided in Tab. I are easily derived. For the purpose of illustration, examples of realizations of Poisson geometries for the case 1 of the benchmark are displayed in Fig. 1 for the $1d$ slab tessellations, the $2d$ extruded tessellations and the $3d$ tessellations.

IV. SIMULATION PARAMETERS

The reference solutions for the ensemble-averaged scalar particle flux $\langle\varphi(x)\rangle$ and the currents $\langle R\rangle$ and $\langle T\rangle$ have been computed as follows. For each benchmark case and sub-case, a large number M of geometries has been generated, and the material properties have been attributed to each volume as described above. Then, for each realization k of the ensemble, linear particle transport has been simulated by resorting to the production Monte Carlo code Tripoli-4®, developed at CEA [11]. The number of simulated particle histories per configuration is 10^6. For a given physical observable O, the benchmark solution is obtained as the ensemble average

$$\langle O\rangle = \frac{1}{M}\sum_{k=1}^{M} O_k \tag{5}$$

where O_k is the Monte Carlo estimate for the observable O obtained for the k-th realization. Depending on the correlation lengths and on the volumetric fractions, the physical observables might display a larger or smaller dispersion around

their average values. For $1d$ slab tessellations, we have taken $M = 10^4$; for the $2d$ extruded tessellations, we have taken $M = 4 \times 10^3$; finally, for the $3d$ tessellations we have taken $M = 10^3$. As a general remark, increasing the dimension implies an increasing computational burden (each realization takes longer both for generation and for Monte Carlo transport), but also a better statistical mixing (a single realization is more representative of the average behaviour). For reference, we have also computed transport results in configurations obeying the atomic mix approximation [3]: the findings corresponding to Poisson tessellations will be contrasted to those coming from the atomic mix model.

1. Computational time

For the simulations discussed here we have largely benefited from a feature that has been recently implemented in the code TRIPOLI-4®, namely the possibility of reading precomputed connectivity maps for the volumes composing the geometry. During the generation of the Poisson tessellations, care has been taken so as to store the indexes of the neighbouring volumes for each realization, which means that during the geometrical tracking a particle will have to find the following crossed volume in a list that might be considerably smaller than the total number of random volumes composing the box (depending on the features of the random geometry). To provide an example, a typical realization of a $3d$ geometry for case 1 will be composed of $\sim 10^5$ volumes, whereas the typical number of neighbours for each volume will of the order of ~ 10. When fed to the transport code, such connectivity maps allow thus for considerable speed-ups for the most fragmented geometries, up to one hundred.

Transport calculations have been run on a cluster based at CEA, with Xeon E5-2680 V2 2.8 GHz processors. An overview of the average computer time $\langle t \rangle$ for each benchmark configuration is provided in Tab. III. Dispersions $\sigma[t]$ are also given. While an increasing trend for $\langle t \rangle$ as a function of dimension is clearly apparent, subtle effects due to correlation lengths and volume fractions for the material compositions come also into play, and strongly influence the average computer time. For some configurations, the dispersion $\sigma[t]$ may become very large, and even be comparable to the average $\langle t \rangle$. Atomic mixing simulations are based on a single homogenized realization, and the dispersion is thus trivially zero.

V. ANALYSIS OF MONTE CARLO SIMULATION RESULTS

1. Transmission, reflection and integral flux

The simulation results for the ensemble-averaged transmission coefficient $\langle T \rangle$, the reflection coefficient $\langle R \rangle$ and the integral flux $\langle \varphi \rangle = \langle \int \int \varphi(\mathbf{r}, \boldsymbol{\omega}) d\boldsymbol{\omega} d\mathbf{r} \rangle$ are provided in Tabs. IV to VI for all the benchmark configurations of *suite* I. Atomic mix results have been also given for reference. For each Monte Carlo transport simulation, the error on the estimated observable was significantly lower than 1%.

The computed values for the $1d$ slab configurations and the atomic mix approximation are in excellent agreement (typically to two or three digits) with those previously reported in [1, 2, 4], and allow concluding that our choice for the benchmark specifications is coherent. For all examined cases, the atomic mix approximation generally yields poor results as compared with the benchmark solutions, and in some cases the discrepancy can add up to several orders of magnitude. In addition, the atomic mix solutions for several cases are strictly identical, since the ensemble-averaged total and scattering cross sections are identical by design. Concerning the benchmark solutions in dimension $d = 1, 2$ and 3, the impact of dimension on the transmission and reflection coefficient is stronger between $d = 1$ and $d = 2$ than between $d = 2$ and $d = 3$, as expected on physical grounds, and has a large variability between cases. The reflection coefficient $\langle R \rangle$ in $d = 1$ is always larger than those in $d = 2, 3$. The transmission coefficient $\langle T \rangle$ is also generally larger, apart from cases $1a$, $1c$, and $3a$, where it is smaller.

2. Distributions of transmission and reflection coefficients

In order to better assess the variability of the transmission and reflection coefficients around their average values, we have also computed their full distributions based on the available realizations in the generated ensembles. The resulting normalized histograms are illustrated in Figs. 2 to 4. As a general consideration, the dispersion of the observables decreases with increasing dimension: the mixing is increasingly efficient and the distribution is more peaked around the average, which is expected on physical grounds. However, even for $d = 3$ it is apparent that several configurations display highly non-symmetrical shapes, and possible cut-offs due to finite-size effects. Especially in $d = 1$, bi-modality may also arise for cases 2 and 3, which is due to the aforementioned effect of random geometries being entirely filled with either material α or β: the peaks observed in the distributions correspond to the values of the transmission or reflection coefficient associated to a fully red or fully blue realization. (The data sets of the distributions are available from the authors upon request.) For the $1d$ slab tessellations, the variances of the transmission and reflection coefficient have been numerically computed in [1]: the values obtained in our simulations are in excellent agreement with those previously reported.

VI. CONCLUSIONS

The key goal of this work was to compute reference solutions for linear transport in stochastic geometries. In order to establish a proper and easily reproducible framework, we have built our specifications upon the benchmark originally proposed by Adams, Larsen and Pomraning, and recently revisited by Brantley. We have thus considered a box of fixed side, with two free surfaces on opposite sides, and reflecting boundary conditions everywhere else. As a prototype example of stochastic media, we have adopted Markov geometries with binary mixing: such geometries have been numerically implemented by resorting to the algorithm for colored Poisson geometries.

Three kinds of Poisson tessellations of the box have been tested: $1d$ slab tessellations, $2d$ extruded tessellations, and full

	Case:	1a	1b	1c	2a	2b	2c	3a	3b	3c
Atomic mixing	$\langle t \rangle$	122	41	65	67	40	66	117	39	66
$d = 1$	$\langle t \rangle$	155	63	117	94	62	75	138	45	69
	$\sigma[t]$	48	16	25	61	14	7	53	6	6
$d = 2$	$\langle t \rangle$	168	77	186	91	62	82	152	46	72
	$\sigma[t]$	9	4	50	26	7	8	54	4	5
$d = 3$	$\langle t \rangle$	3962	1711	3582	119	63	87	144	46	75
	$\sigma[t]$	889	364	862	36	4	4	35	3	4

TABLE III. Simulation times t for the benchmark configurations, expressed in seconds. The cases of *suite* I.

3d tessellations. To the best of our knowledge, benchmark solutions for 2d and 3d tessellations with Markov mixing have never been studied before. Material compositions and correlation lengths, as well as source and boundary conditions, have been assigned based on the benchmark specifications. A large number of random geometries and material compositions have been realized. For each realization, mono-energetic linear transport with isotropic scattering and absorption has been simulated by Monte Carlo method. The code TRIPOLI-4® developed at CEA has been used for this purpose.

The physical observables that have been examined in this work are the reflection and transmission coefficients, and the scalar particle flux, averaged over the ensemble of available realizations. The full distributions of the reflection and transmission coefficients have been also examined, in order to evaluate the impact of correlation lengths and volumetric fractions on the dispersion of these observables around their average values.

VII. ACKNOWLEDGMENTS

The authors wish to thank Électricité de France (EDF) for partial financial support.

REFERENCES

1. M. ADAMS, E. LARSEN, and G. POMRANING, "Benchmark results for particle transport in a binary Markov statistical medium," *Journal of Quantitative Spectroscopy and Radiation Transfer*, **42**, 253–266 (1989).
2. P. BRANTLEY, "A benchmark comparison of Monte Carlo particle transport algorithms for binary stochastic mixtures," *Journal of Quantitative Spectroscopy and Radiation Transfer*, **112**, 599–618 (2011).
3. G. POMRANING, *Linear kinetic theory and particle transport in stochastic mixtures*, World Scientific Publishing, River Edge, NJ, USA (1991).
4. O. ZUCHUAT, R. SANCHEZ, I. ZMIJAREVIC, and F. MALVAGI, "Transport in renewal statistical media: benchmarking and comparison with models," *Journal of Quantitative Spectroscopy and Radiation Transfer*, **51**, 689–722 (1994).
5. G. ZIMMERMAN and M. ADAMS, "Algorithms for Monte Carlo particle transport in binary statistical mixtures," *Transactions of the American Nuclear Society*, **66**, 287 (1991).
6. L. SANTALÓ, *Integral geometry and geometric probability*, Addison-Wesley, Reading, MA, USA (1976).
7. P. SWITZER, "Random set process in the plane with Markov property," *Annals of Mathematical Statistics*, **36**, 1859–1863 (1965).
8. A. AMBOS and G. MIKHAILOV, "Statistical simulation of an exponentially correlated many-dimensional random field," *Russian Journal of Numerical Analysis and Mathematical Modelling*, **26**, 263–273 (2011).
9. T. LEPAGE, L. DELABY, F. MALVAGI, and A. MAZZOLO, "Monte Carlo simulation of fully Markovian stochastic geometries," *Progress in Nuclear Science and Technology*, **2**, 743–748 (2011).
10. C. LARMIER, E. DUMONTEIL, F. MALVAGI, A. MAZZOLO, and A. ZOIA, "Finite-size effects and percolation properties of Poisson geometries," *Physical Review E*, **94**, 012130 (2016).
11. E. BRUN, F. DAMIAN, C. DIOP, E. DUMONTEIL, F.-X. HUGOT, C. JOUANNE, Y.-K. LEE, F. MALVAGI, A. MAZZOLO, O. PETIT, J.-C. TRAMA, T. VISONNEAU, and A. ZOIA, "TRIPOLI-4, CEA, EDF and AREVA reference Monte Carlo code," *Annals of Nuclear Energy*, **82**, 151–160 (2015).

Configuration	Observable	Atomic mixing	1d	2d	3d
1a	$\langle R \rangle$	0.4919 ± 0.0004	0.435 ± 0.002	0.4031 ± 0.0006	0.4065 ± 0.0004
	$\langle T \rangle$	$0.00484 \pm 7 \times 10^{-5}$	0.0147 ± 0.0002	0.0173 ± 0.0001	0.0162 ± 0.0001
	$\langle \varphi \rangle$	5.499 ± 0.007	6.09 ± 0.01	6.356 ± 0.008	6.318 ± 0.008
1b	$\langle R \rangle$	0.0193 ± 0.0001	0.0841 ± 0.0007	0.0453 ± 0.0002	0.0376 ± 0.0002
	$\langle T \rangle$	$8 \times 10^{-6} \pm 3 \times 10^{-6}$	0.0017 ± 0.0001	$0.00108 \pm 3 \times 10^{-5}$	$0.00085 \pm 3 \times 10^{-5}$
	$\langle \varphi \rangle$	1.077 ± 0.001	2.89 ± 0.02	2.165 ± 0.005	1.920 ± 0.003
1c	$\langle R \rangle$	0.4747 ± 0.0004	0.4743 ± 0.0004	0.4059 ± 0.0004	0.4036 ± 0.0004
	$\langle T \rangle$	$0.00384 \pm 6 \times 10^{-5}$	0.0159 ± 0.0003	0.0179 ± 0.0001	0.0164 ± 0.0001
	$\langle \varphi \rangle$	5.172 ± 0.0007	6.95 ± 0.03	6.52 ± 0.01	6.296 ± 0.0008

TABLE IV. Ensemble-averaged observables for the benchmark configurations: *suite* I - case 1.

Configuration	Observable	Atomic mixing	1d	2d	3d
2a	$\langle R \rangle$	0.4919 ± 0.0004	0.235 ± 0.003	0.226 ± 0.002	0.223 ± 0.002
	$\langle T \rangle$	$0.00484 \pm 7 \times 10^{-5}$	0.0975 ± 0.0009	0.0955 ± 0.0007	0.0935 ± 0.0008
	$\langle \varphi \rangle$	5.499 ± 0.007	7.63 ± 0.02	7.57 ± 0.01	7.55 ± 0.02
2b	$\langle R \rangle$	0.0193 ± 0.0001	0.285 ± 0.0002	0.196 ± 0.001	0.161 ± 0.002
	$\langle T \rangle$	$8 \times 10^{-6} \pm 3 \times 10^{-6}$	0.193 ± 0.003	0.143 ± 0.002	0.119 ± 0.002
	$\langle \varphi \rangle$	1.077 ± 0.001	11.65 ± 0.08	9.00 ± 0.06	7.76 ± 0.07
2c	$\langle R \rangle$	0.4747 ± 0.0004	0.4304 ± 0.0008	0.3669 ± 0.0006	0.3438 ± 0.0006
	$\langle T \rangle$	$0.00384 \pm 6 \times 10^{-5}$	0.185 ± 0.002	0.176 ± 0.002	0.165 ± 0.0002
	$\langle \varphi \rangle$	5.172 ± 0.007	12.50 ± 0.06	11.39 ± 0.05	10.76 ± 0.06

TABLE V. Ensemble-averaged observables for the benchmark configurations: *suite* I - case 2.

Configuration	Observable	Atomic mixing	1d	2d	3d
3a	$\langle R \rangle$	0.7820 ± 0.0004	0.693 ± 0.003	0.672 ± 0.003	0.670 ± 0.004
	$\langle T \rangle$	0.0667 ± 0.0003	0.161 ± 0.002	0.170 ± 0.002	0.169 ± 0.003
	$\langle \varphi \rangle$	14.83 ± 0.02	16.35 ± 0.05	16.46 ± 0.05	16.35 ± 0.08
3b	$\langle R \rangle$	$0.00202 \pm 4 \times 10^{-5}$	0.0349 ± 0.0004	0.0221 ± 0.0004	0.0167 ± 0.0006
	$\langle T \rangle$	$9 \times 10^{-6} \pm 3 \times 10^{-6}$	0.0740 ± 0.002	0.061 ± 0.002	0.045 ± 0.003
	$\langle \varphi \rangle$	1.004 ± 0.001	5.01 ± 0.06	4.08 ± 0.06	3.49 ± 0.08
3c	$\langle R \rangle$	0.4747 ± 0.0004	0.443 ± 0.001	0.406 ± 0.001	0.395 ± 0.001
	$\langle T \rangle$	$0.00384 \pm 6 \times 10^{-5}$	0.101 ± 0.002	0.098 ± 0.002	0.085 ± 0.003
	$\langle \varphi \rangle$	5.172 ± 0.007	8.80 ± 0.07	8.34 ± 0.07	7.9 ± 0.1

TABLE VI. Ensemble-averaged observables for the benchmark configurations: *suite* I - Case 3.

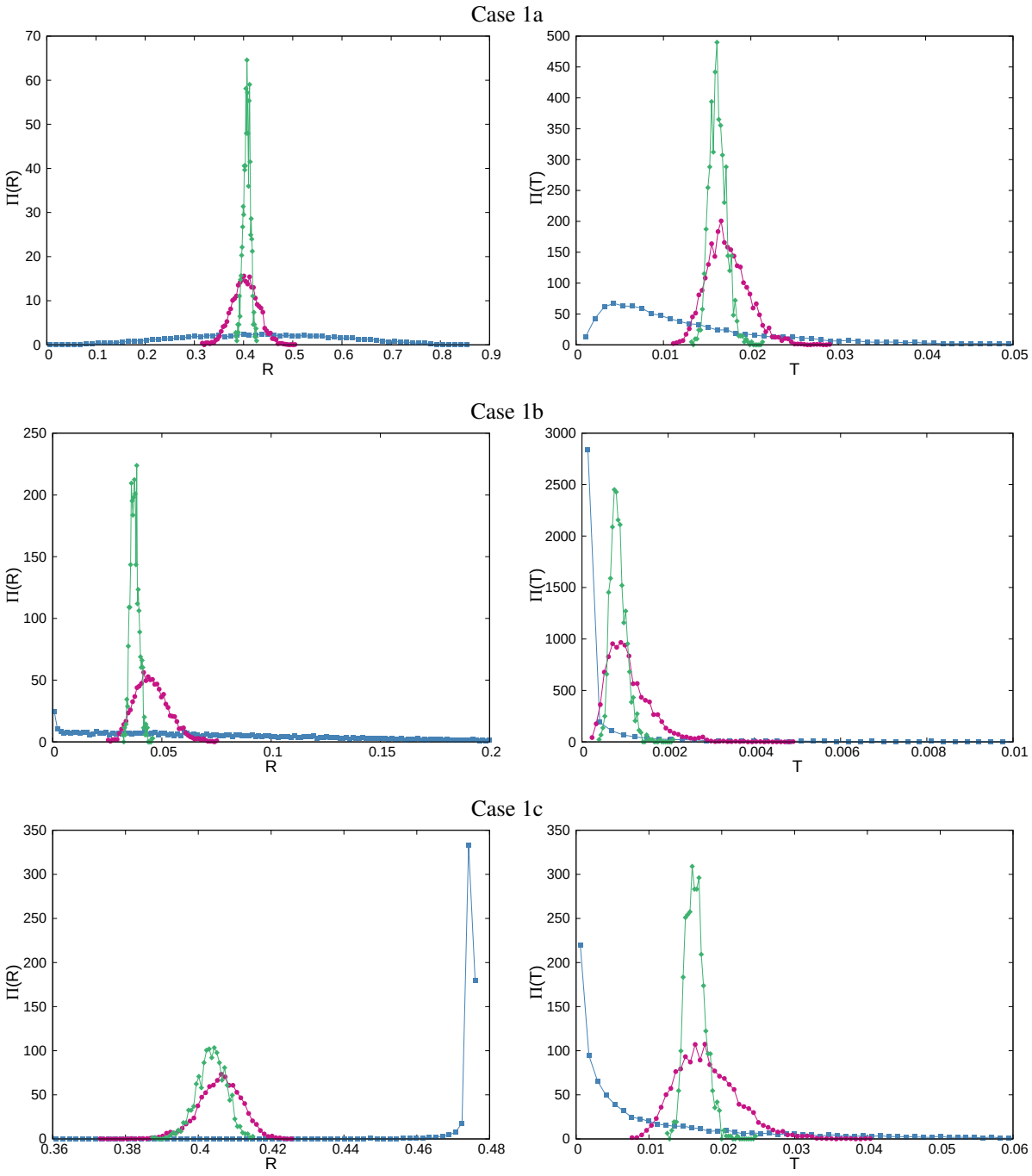

Fig. 2. Left column: normalized distributions $\Pi(R)$ of the reflection coefficients R; right column: normalized distributions $\Pi(T)$ of the transmission coefficients T. *Suite* I configurations, case 1. Blue squares represent the 1d slab tessellations, red circles the 2d extruded tessellations, and green diamonds the 3d tessellations.

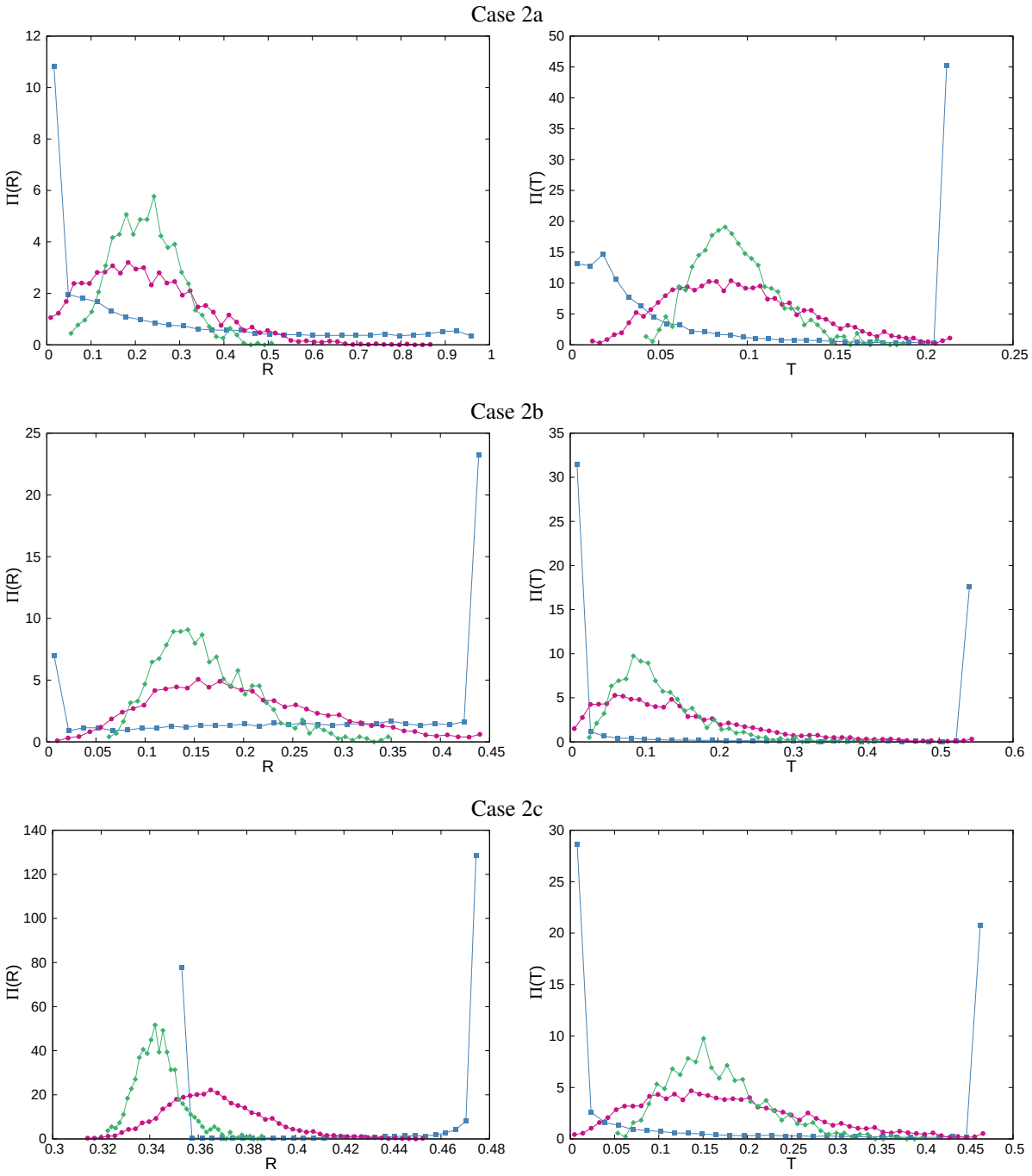

Fig. 3. Left column: normalized distributions $\Pi(R)$ of the reflection coefficients R; right column: normalized distributions $\Pi(T)$ of the transmission coefficients T. *Suite* I configurations, case 2. Blue squares represent the 1d slab tessellations, red circles the 2d extruded tessellations, and green diamonds the 3d tessellations.

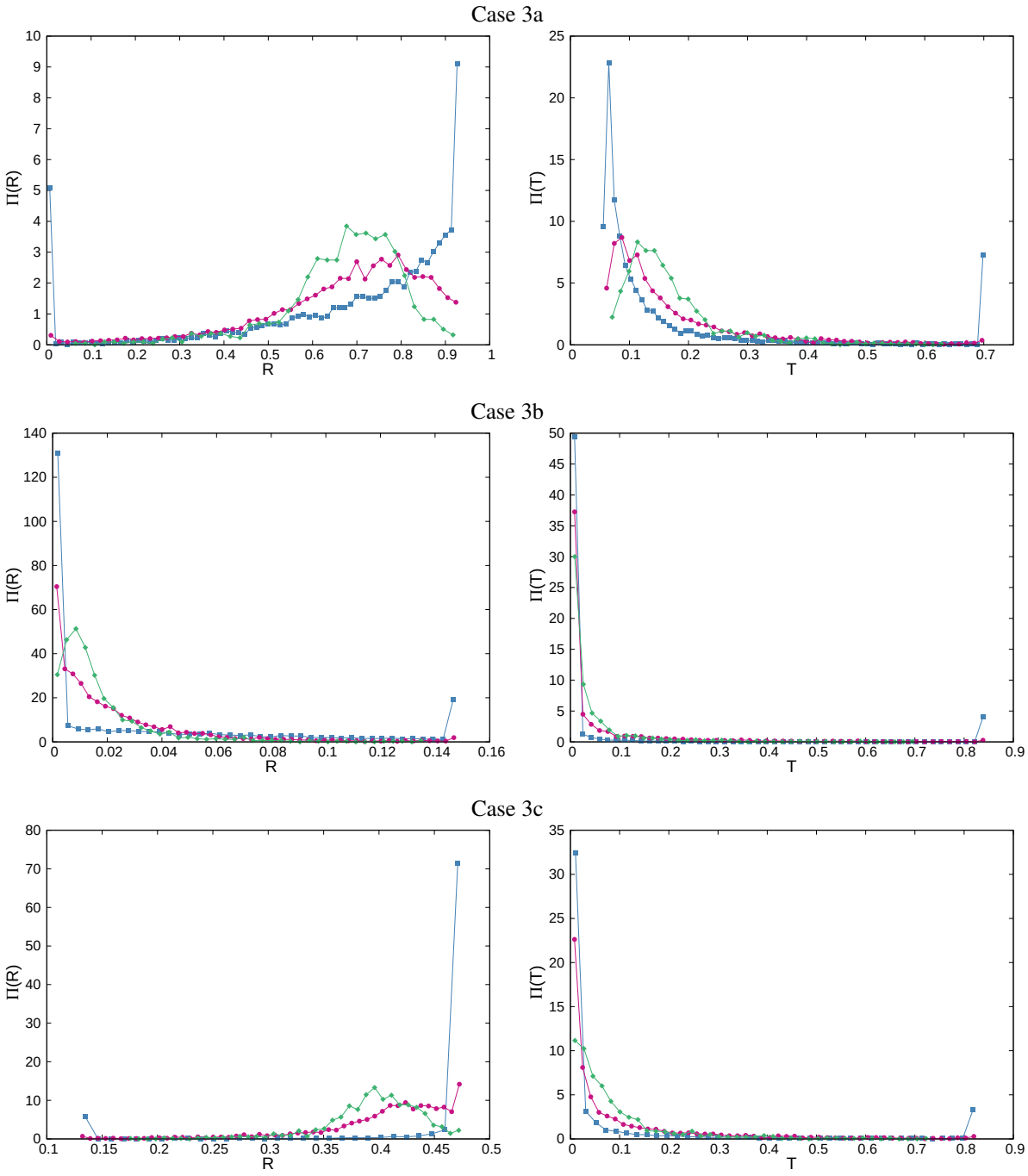

Fig. 4. Left column: normalized distributions $\Pi(R)$ of the reflection coefficients R; right column: normalized distributions $\Pi(T)$ of the transmission coefficients T. *Suite* I configurations, case 3. Blue squares represent the 1d slab tessellations, red circles the 2d extruded tessellations, and green diamonds the 3d tessellations.